Dirac optical potentials constrained by a Dirac-Hartree approach to nuclear structure

S. Hama

Theoretical Physics Institute, Department of Physics, University of Alberta, Edmonton, Alberta, Canada T6G 2J1

B. C. Clark, R. E. Kozack,* and S. Shim

Department of Physics, The Ohio State University, Columbus, Ohio 43210

E. D. Cooper

Department of Physics, McGill University, Montreal, Quebec, Canada H3A 2T8

R. L. Mercer

Thomas J. Watson Research Center, Yorktown Heights, New York 10598

B. D. Serot

Department of Physics, Indiana University, Bloomington, Indiana 47405

Lorentz scalar and four-vector optical potentials are obtained for protons elastically scattered from ^{16}O, ^{40}Ca, ^{48}Ca, ^{90}Zr, and ^{208}Pb. It is demonstrated that Dirac optical potentials constrained by relativistic Hartree theory are capable of producing good agreement with experiment.

I. INTRODUCTION

The rapid development of relativistic treatments of nuclear reactions and nuclear structure over the past few years has increased the interest in phenomenological optical potentials appropriate for use in the Dirac equation. In this paper we present the results of an analysis of a large body of experimental data for proton-nucleus elastic scattering. The resulting optical potentials are consistent with the theoretical ideas behind the use of the Dirac equation as the relevant wave equation for describing nuclear reactions. In particular, we constrain the real parts of the optical potentials by relativistic Dirac-Hartree calculations.[1-3] The analysis presented here provides a test of this constraint for a wide range of projectile energies and for a number of spin-zero targets. We also seek evidence for global parametrizations of the Dirac potentials by studying the energy dependence of the potential parameters.

In the next section we describe the construction of the relativistic Hartree optical model potentials. Section III gives the results of our analysis of elastic scattering cross sections and spin observables, together with a discussion of the characteristic features of the scalar and vector Dirac optical potentials and the Schrödinger equivalent potentials obtained from them.[2] In Sec. IV we present our conclusions and suggestions for further work.

II. CALCULATION OF THE REAL PART OF THE OPTICAL POTENTIAL

The real part of the nucleon-nucleus optical potential is calculated using the Dirac-Hartree approach of Ref. 1. The reader is referred to that work for details; here we summarize briefly the results as they pertain to the present calculation.

The Dirac-Hartree equations for a finite nucleus may be derived from a model relativistic Lagrangian density using either Green's function techniques[1] or a product of single-particle Dirac wave functions as the ground state.[4] As a prototype, consider the model of Walecka,[5] for which

$$\mathcal{L} = \mathcal{L}_0 + g_s \bar{\psi}\psi\phi - g_v \bar{\psi}\gamma_\mu \psi V^\mu , \quad (1)$$

where $\mathcal{L}_0$ is the noninteracting Lagrangian density for baryon (ψ), scalar meson (ϕ), and vector meson (V_μ) fields. (The results presented below use an extended model that includes additional boson degrees of freedom.[6]) In the Green's function approach, the Hartree approximation includes self-consistently the iterated direct ("tadpole") interactions between nucleons in the baryon and meson propagators and the energy density. This is illustrated in Fig. 1. In the wave-function approach, one begins with the field equations derived from (1) and replaces the meson field operators with static, classical fields. In addition, the baryon densities (which serve as source terms in the meson field equations) are evaluated approximately as sums over single-particle wave functions.

Both of the preceding techniques lead to a set of coupled, nonlinear differential equations for the classical meson fields and single-nucleon wave functions. If we write the static four-component Dirac wave functions as[7]

$$\psi_\alpha(\mathbf{x}) \equiv \psi_{n\kappa m t}(\mathbf{x}) = \begin{bmatrix} i\dfrac{G_{n\kappa t}(r)}{r}(r)\Phi_{\kappa m}\eta_t \\ -\dfrac{F_{n\kappa t}(r)}{r}\Phi_{-\kappa m}\eta_t \end{bmatrix} , \quad (2)$$

where $\Phi_{\kappa m}$ are spin-$\frac{1}{2}$ spherical harmonics labeled by κ and m, and η_t are isospinors labeled by t, one finds

$$\frac{d}{dr}G_\alpha(r)+\frac{\kappa}{r}G_\alpha(r)-[E_\alpha-U_0(r)-V_c(r)+M+U_s(r)]F_\alpha(r)=0 \ ,$$ (3a)

$$\frac{d}{dr}F_\alpha(r)-\frac{\kappa}{r}F_\alpha(r)+[E_\alpha-U_0(r)-V_c(r)-M-U_s(r)]G_\alpha(r)=0 \ .$$ (3b)

Here U_0, V_c, and U_s are the four vector, coulomb, and scalar potentials, respectively, and we have assumed spherical symmetry, as appropriate for a doubly magic nucleus. The meson potentials are determined self-consistently by solving additional differential equations driven by the baryon densities. For example, the scalar meson field U_s satisfies

$$\frac{d^2}{dr^2}U_s(r)+\frac{2}{r}\frac{d}{dr}U_s(r)-m_s^2U_s(r)=g_s^2\rho_s(r)=g_s^2\sum_\alpha^{\text{occupied}}\left[\frac{2j_\alpha+1}{4\pi r^2}\right][\,|\,G_\alpha(r)\,|^2-|\,F_\alpha(r)\,|^2\,] \ ,$$ (4)

where m_s is the scalar meson mass. The vector potential U_0 contains contributions from both isoscalar (ω) and isovector (ρ) mesons, as determined by similar equations driven by the baryon density (proportional to $|\,G_\alpha\,|^2+|\,F_\alpha\,|^2$). The coulomb potential V_c satisfies Poisson's equation, of course. (For the full set of equations in the present model, see Ref. 1.)

These field equations determine the meson potentials and single-particle nucleon wave functions in this model and depend on four parameters: g_s,g_v,g_ρ (the rho meson coupling to nucleons), and m_s. We consider the parameters $M=939$ MeV, $m_v \equiv m_\omega=783$ MeV, $m_\rho=770$ MeV, and $\alpha=e^2/4\pi\simeq\frac{1}{137}$ fixed at their experimental values. The remaining four free parameters are normalized as far as possible to the bulk properties of nuclear matter, as discussed in Ref. 1, and take the values $g_s^2=109.63$, $g_V^2=190.43$, $g_\rho^2=65.226$, and $m_s=520$ MeV. These values lead to an accurate description of charge densities, neutron densities, rms radii, and single-nucleon energy levels for doubly magic nuclei throughout the periodic table.

To utilize the preceding results in the relativistic optical model formalism, we assume that the *geometries* of the real parts of the nucleon-nucleus optical potential for medium- and high-energy incident nucleons are given by the bound-state Dirac-Hartree solutions U_0, U_s, and V_c. Since the Hartree approximation results in state- (or energy-) independent potentials, the energy dependence is specified in the present work by overall scale parameters determined by the fitting procedure, as discussed below. More sophisticated approximations for the nuclear ground state lead naturally to state-dependent meson potentials.[4] In addition, to account for the finite-size effects of the nucleons themselves (which are also neglected in the Hartree approximation), we determine the optical potentials by folding over a suitable single-nucleon form factor. This is done in the following fashion.

Consider the scalar optical potential U_s^{opt} generated from the folding integral

$$U_s^{\text{opt}}(r)=\int d\mathbf{r}'d\mathbf{r}_1 d\mathbf{r}_2 \rho_b(\,|\,\mathbf{r}-\mathbf{r}'\,|\,)v_s(\,|\,\mathbf{r}'-\mathbf{r}_1\,|\,)\rho_{b'}(\,|\,\mathbf{r}_1-\mathbf{r}_2\,|\,)\rho_s^{\text{Hartree}}(r_2) \ .$$ (5)
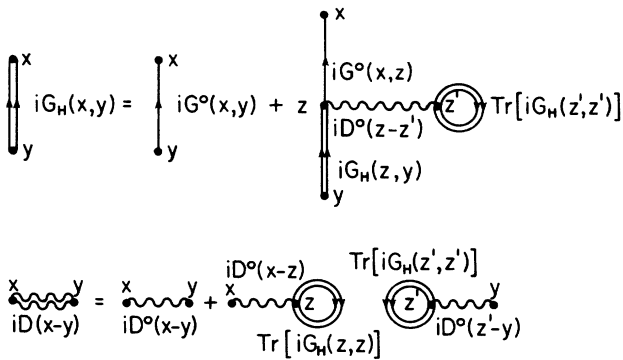
FIG. 1. Diagrammatic Dirac-Hartree representation for the baryon and meson propagators. Here G° is the noninteracting baryon propagator at finite density and G_H is the Hartree propagator. Thus, the first set of diagrams represents an integral equation for G_H. Results are shown here for scalar mesons; there is a corresponding contribution for each exchanged boson. Note that the Hartree propagator G_H is defined using the noninteracting boson propagator D°. The corresponding "tadpole" contributions are to be included in the Dirac-Hartree energy density.

This is pictorially illustrated in Fig. 2(a), which shows the incident nucleon interaction with all nucleons in the target nucleus. Here ρ_b and $\rho_{b'}$ are single-nucleon form factors, $v_s(r)$ is the static Yukawa meson propagator, and $\rho_s^{\text{Hartree}}(r)$ is the scalar meson density generated by the
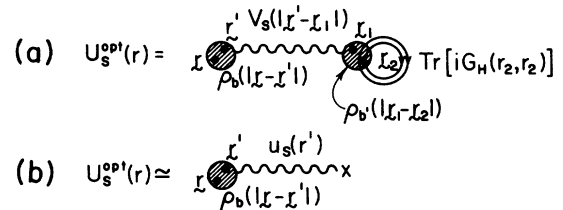
FIG. 2. Diagrammatic representation of the nucleon-nucleus optical potential for scalar meson exchange [Eq. (5)]. In (a), the blobs represent single-nucleon form factors, $v_s(r)$ is the static Yukawa meson propagator, and the loop containing G_H generates the scalar density of baryons. The integral over the scalar propagator and density gives the Hartree potential, as indicated in (b).

tadpole loop [or, equivalently, the sum on single-nucleon wave functions in Eq. (4)]. This folding procedure is slightly different from that used in Ref. 3, but allows us to separate the effects of incident and target nucleons more easily. Relations analogous to (5) define the Lorentz vector optical potential U_0^{opt} and, of course, these lowest-order potentials are summed to all orders by solving the Dirac equation for the four-component scattering-state wave function.

In principle, the form factors ρ_b and $\rho_{b'}$ should be used in the static calculation of the Hartree potentials for bound nucleons. Instead, since the Hartree potentials are calculated self-consistently with no form factors, we set $\rho_{b'}(r) = \delta^{(3)}(\mathbf{r})$. It is likely that including additional form factors will have only a small effect on the Hartree potentials or the optical-model analysis, for reasons discussed below. With the preceding replacement, the scalar and vector optical potentials may be written

$$U_{s,0}^{\mathrm{opt}}(r) \approx \int d\mathbf{r}' d\mathbf{r}_1 \rho_b(\,|\,\mathbf{r}-\mathbf{r}'\,|\,) v_{s,0}(\,|\,\mathbf{r}'-\mathbf{r}_1\,|\,) \rho_{s,0}^{\mathrm{Hartree}}(r_1)$$

$$= \int d\mathbf{r}' \rho_b(\,|\,\mathbf{r}-\mathbf{r}'\,|\,) U_{s,0}(r') \, , \qquad (6)$$

where the last line follows from the solution to Eq. (4) and is represented in Fig. 2(b). The nucleon-nucleus optical potential is therefore determined by folding the calculated Hartree potentials with a suitable form factor for the projectile nucleon. The detailed form of ρ_b is unimportant, as long as the nucleon rms radius is approxi-
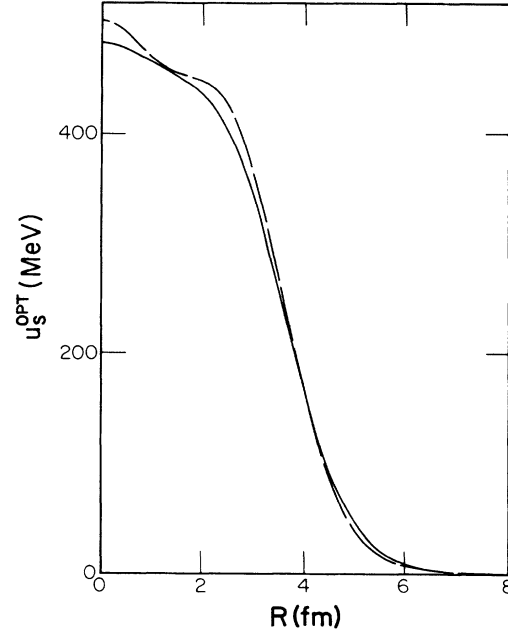
FIG. 3. The Hartree potential U_s (dashed) and scalar optical potential U_s^{opt} (solid) for ^{40}Ca. The latter is evaluated with the exponential form factor in Eq. (7a). Results calculated with the Gaussian form factor (7b) are too similar to be distinguished on this graph.

TABLE I. Values of C_v and C_s determined by the fitting procedure and the volume integrals of the real and imaginary effective central and spin-orbit potentials.

A	T_p(MeV)	C_v	C_s	Central (MeV fm^3) Re(J/A)	(MeV fm^3) Im(J/A)	SO (MeV fm^3) Re($K/A^{1/3}$)	Im($K/A^{1/3}$)
16	200.0	0.736	0.763	−122.1	−161.2	−80.3	7.6
16	613.0	0.510	0.600	95.3	−219.8	−36.6	13.3
16	800.0	0.498	0.652	64.2	−451.8	−45.9	9.6
40	26.3	0.663	0.695	−377.9	−94.1	−98.0	3.2
40	40.0	0.662	0.698	−360.8	−93.9	−96.1	9.8
40	181.3	0.603	0.635	−118.2	−142.9	−69.6	18.6
40	200.0	0.606	0.638	−93.9	−149.8	−68.8	6.3
40	300.0	0.537	0.602	−49.5	−200.9	−54.9	8.5
40	400.0	0.480	0.579	−43.7	−250.8	−43.5	4.1
40	497.5	0.493	0.595	39.7	−252.5	−41.2	13.8
40	613.0	0.388	0.463	95.5	−252.2	−28.1	11.6
40	800.0	0.402	0.537	106.9	−340.1	−26.2	10.2
48	30.0	0.678	0.710	−363.6	−96.7	−100.1	2.9
48	40.0	0.597	0.641	−347.9	−97.7	−86.5	2.6
48	497.5	0.454	0.545	46.5	−242.1	−37.2	16.3
48	800.0	0.365	0.488	103.4	−338.6	−23.6	8.8
90	160.0	0.617	0.654	−138.0	−147.5	−73.6	27.6
90	182.0	0.467	0.520	−144.9	−150.0	−54.9	15.6
90	500.0	0.517	0.621	74.4	−219.3	−43.0	13.7
90	800.0	0.328	0.446	91.4	−371.6	−21.3	6.6
208	182.0	0.596	0.634	−105.4	−131.7	−70.2	13.7
208	300.0	0.534	0.580	7.6	−156.0	−53.9	4.1
208	400.0	0.508	0.582	44.2	−187.7	−46.5	6.5
208	497.5	0.414	0.479	85.0	−225.2	−33.6	5.2
208	613.0	0.355	0.440	81.6	−240.6	−26.1	11.1
208	800.0	0.412	0.556	138.6	−338.3	−26.7	7.6
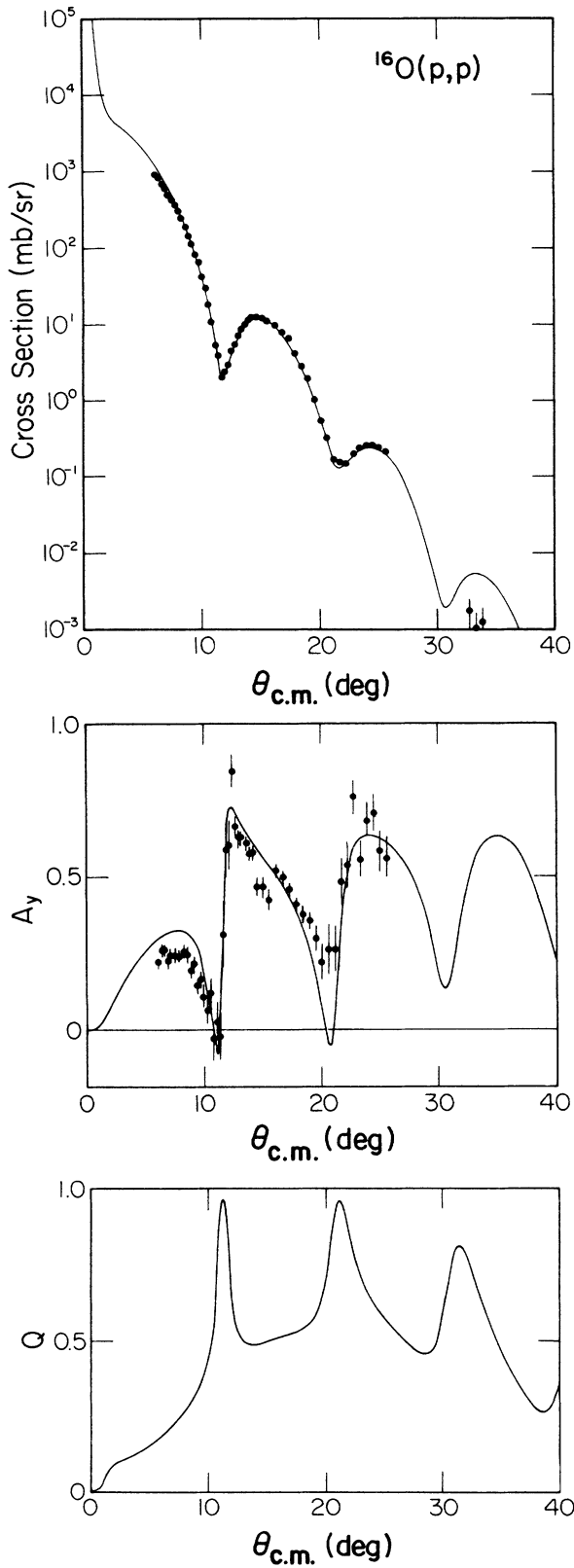
FIG. 4. Calculated observables for 800 MeV protons scattered elastically from ^{16}O. See Ref. 10 for the references to experimental data.
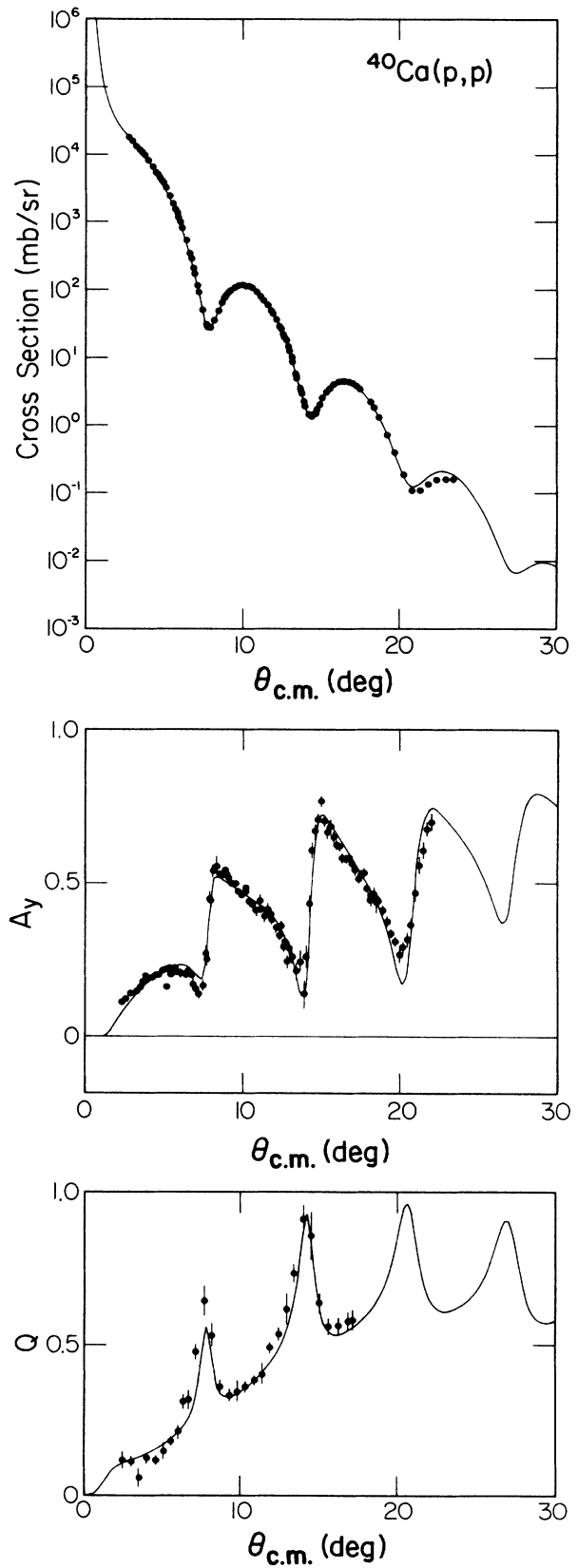
FIG. 5. Calculated observables for 800 MeV protons scattered elastically from ^{40}Ca. See Ref. 10 for the references to experimental data.
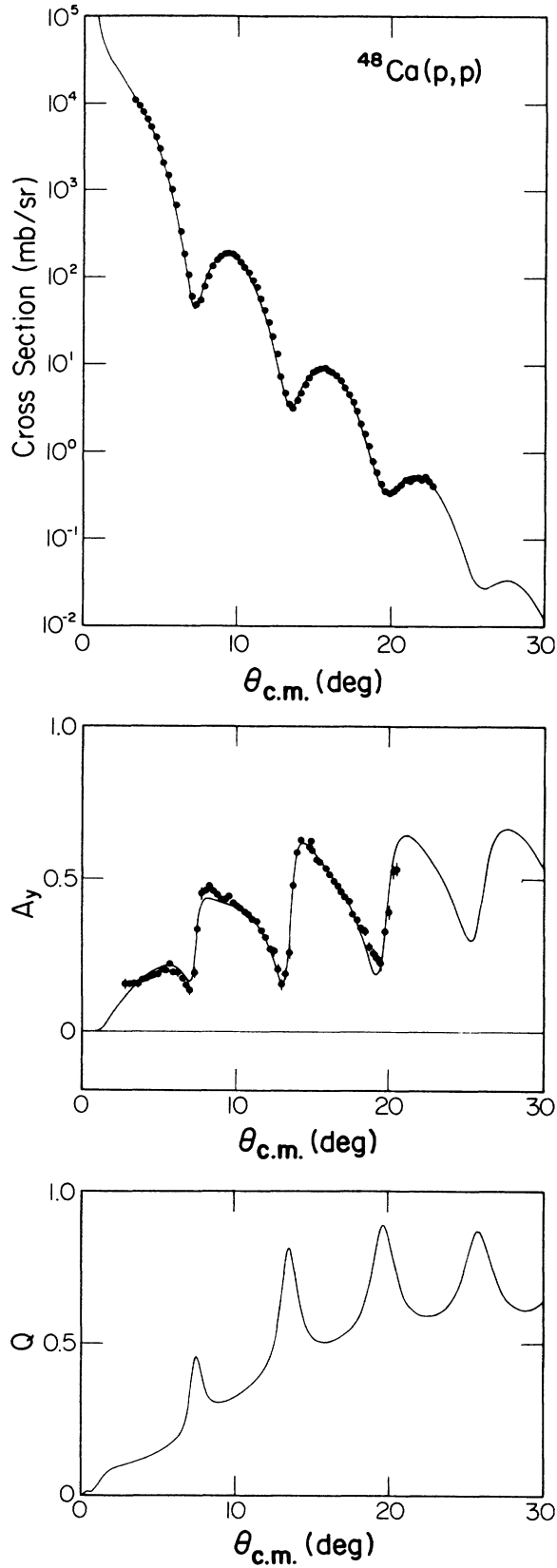
FIG. 6. Calculated observables for 800 MeV protons scattered elastically from ^{48}Ca. See Ref. 10 for the references to experimental data.
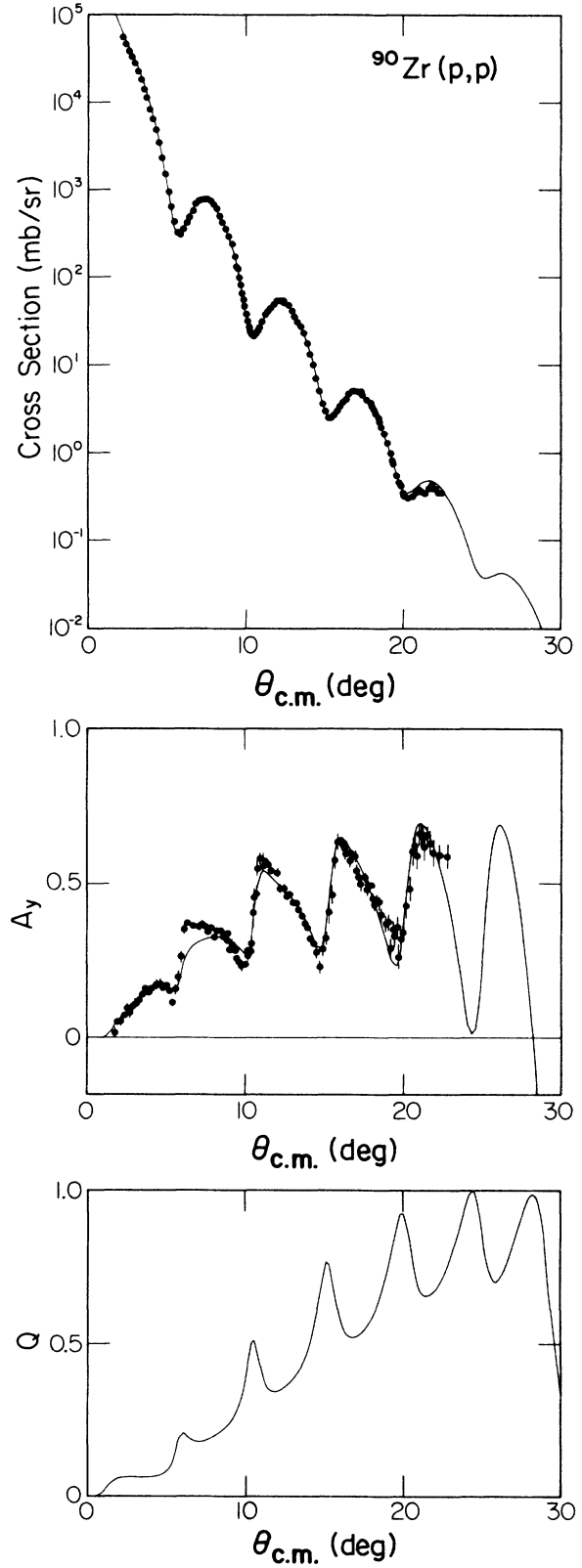
FIG. 7. Calculated observables for 800 MeV protons scattered elastically from ^{90}Zr. See Ref. 10 for the references to experimental data.
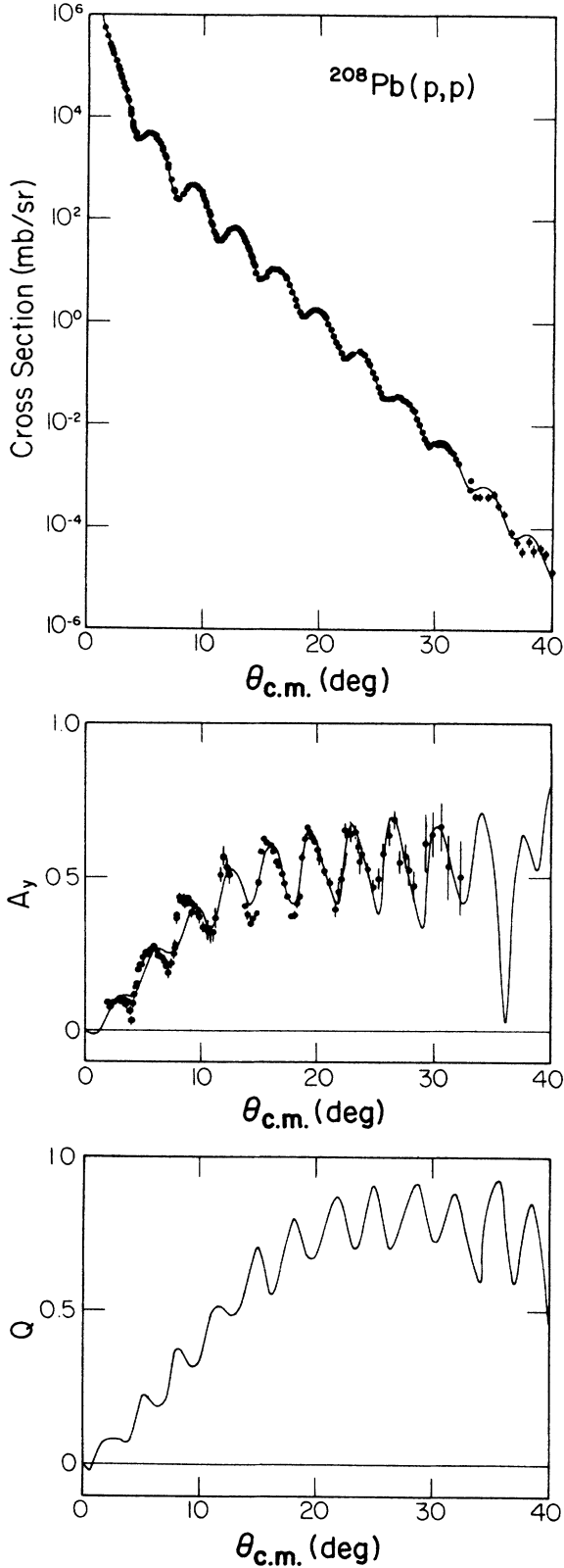
FIG. 8. Calculated observables for 800 MeV protons scattered elastically from ^{208}Pb. See Ref. 10 for the references to experimental data.

mately 0.7–0.9 fm, and similar results were obtained with an exponential form

$$\rho_b^{(1)}(\mathbf{x}) = \frac{\mu^3}{8\pi} e^{-\mu|\mathbf{x}|} , \tag{7a}$$

and a Gaussian form

$$\rho_b^{(2)}(\mathbf{x}) = \frac{\nu^3}{\pi^{3/2}} e^{-\nu^2 \mathbf{x}^2} , \tag{7b}$$

with $\mu = 4.2701$ fm^{-1} and $\nu = 1.5309$ fm^{-1}, yielding rms nucleon radii of 0.81 and 0.80 fm, respectively. Results for the scalar potential for ^{40}Ca are shown in Fig. 3. As further justification for this procedure, note that once details in $U_{s,0}^{\text{opt}}$ on the scale of $\approx \frac{1}{2}$ fm have been "smoothed out" by folding at the projectile vertex, it is unlikely that further "smoothing" at the target vertex will lead to significant changes.

III. ANALYSIS OF EXPERIMENTAL DATA

The motivation for this work was to demonstrate that acceptable fits to proton-nucleus elastic scattering data could be obtained using the optical potentials described in Sec. II. To do this we scale the real optical potentials of Eq. (6) by factors C_v and C_s to include possible sources of the energy dependence in the vector and scalar potentials. The real optical potentials contain only these two parameters; the radial dependence is fixed by the relativistic Hartree calculation. The scalar and vector potentials are given by

$$V_0^{\text{opt}}(r) = C_v U_0^{\text{opt}}(r) + iW_0 f_0(r) , \tag{8a}$$

$$V_s^{\text{opt}}(r) = C_s U_s^{\text{opt}}(r) + iW_s f_s(r) , \tag{8b}$$

where $f(r)$ is a two-parameter Fermi shape. The model contains a total of eight parameters which are varied to obtain fits to experimental data for each energy and each target.

Two different relativistic optical model programs, CZENITH (Ref. 8) and RUNT,[9] were used in the analysis. This provided a check on the searches and on the numerical procedures. We found acceptable fits to the data for all spin-zero, closed-shell targets appropriate for the constraint. We considered ^{16}O, ^{40}Ca, ^{48}Ca, ^{90}Zr, and ^{208}Pb targets at intermediate energies, $T_p \geq 200$ MeV, and ^{40}Ca and ^{48}Ca at a few lower energies. For the data sets used in this work,[10,11] the values of C_v and C_s determined by the fitting procedure and the volume integrals of the real and imaginary effective central and spin-orbit potentials are given in Table I. In Figs. 4–8 we show the results for ^{16}O, ^{40}Ca, ^{48}Ca, ^{90}Zr, and ^{208}Pb at 800 MeV, where experimental data exists for every target considered. These figures are representative of the quality of the fits at all energies. The results show that the procedure used to constrain the optical potential is reasonable. In addition, this work provides a link between the phenomenology and the results of relativistic mean field calculations.

The energy dependence of the effective potentials is smooth, especially for the effective central potential.
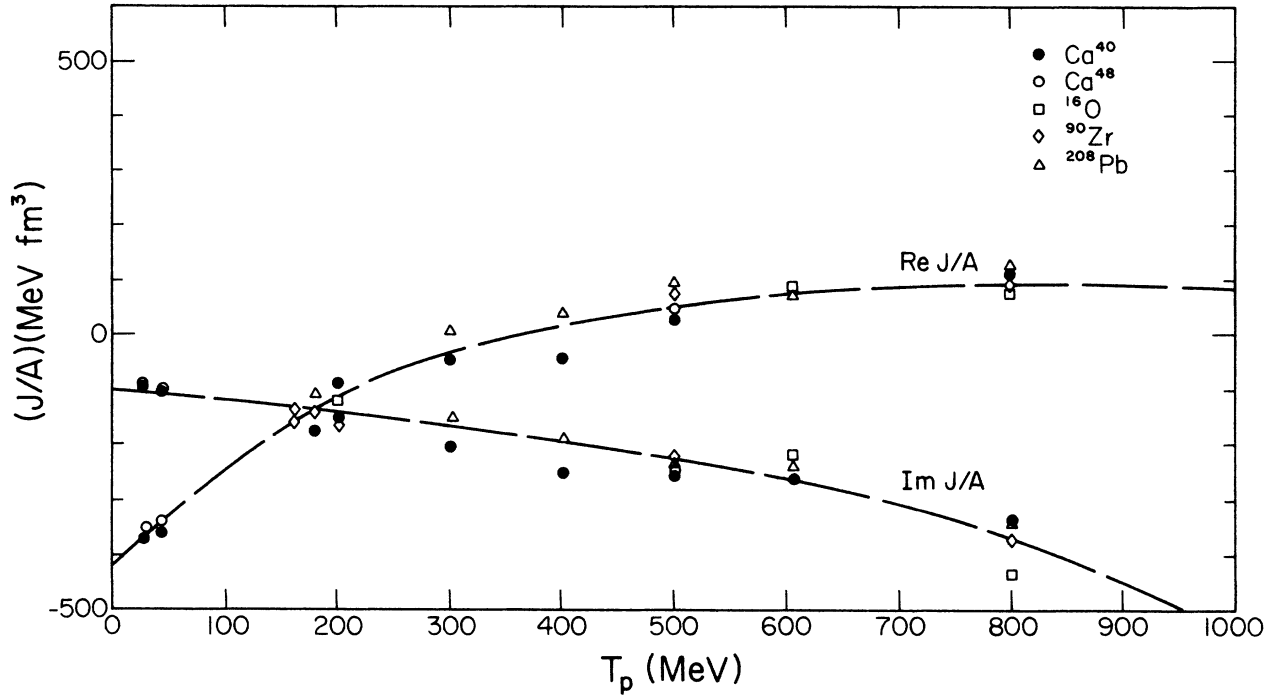
FIG. 9. Real and imaginary effective central volume integrals divided by A as a function of T_p calculated from the scalar and vector Dirac potential determined by the analysis described in the text.

Essentially all of the A dependence can be removed by dividing the volume integral by A (or $A^{1/3}$ for the spin-orbit volume integral). Figures 9 and 10 show the results graphically, and we note that the only significant departure from a smooth energy variation occurs for the spin-orbit potential between 150 and 200 MeV. Such behavior

has been observed in several of analyses of medium-energy data.[10]

Because the energy dependence determined from the single energy fits was, in general, quite reasonable, we sought global parametrizations for the imaginary potential parameters and for C_v and C_s. It is surprising that
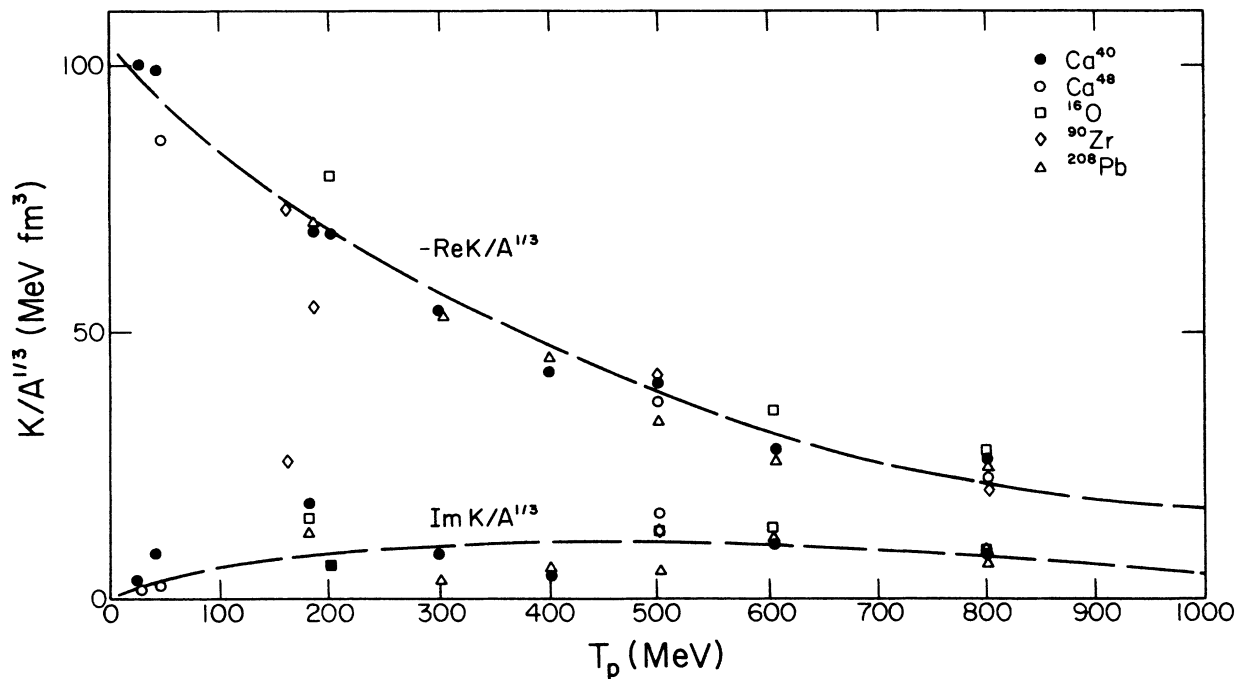
FIG. 10. Real and imaginary effective spin-orbit volume integrals divided by $A^{1/3}$ as a function of T_p calculated from the scalar and vector Dirac potential determined by the analysis described in the text.

the imaginary effective volume integrals exhibit the reasonable energy variation shown in Fig. 9, in view of the change in the imaginary effective potential from volume form to surface-peaked form as the projectile energy decreases. This behavior is accomplished by the strong energy dependence of the imaginary geometry parameters. We conclude that a better parametrization would be a combination of surface and volume geometries. An analysis employing this more general geometry is underway.

Next we examined the energy dependence of the eight parameters varied in the fitting. The lowest energies ($T_p < 100$ MeV) were excluded for the reason discussed above. Several different parametrizations of the energy dependence were considered; however, none of them produced acceptable results. Interpolation was unreliable and extrapolation, as is usually the case for global fits, was very poor. This failure arises from the strong correlations which exist between the parameters. These correlations make it difficult to find simple expressions for the energy dependence of the potential parameters. Although the energy dependence of an individual parameter can be represented by a low order polynomial, when used in conjunction with similar fits for the other parameters, resulting potentials give only qualitative agreement with experiment. This situation can be remedied by considering global fits that use the entire data set for all energies simultaneously. The expansion of the data set from a few hundred points to several thousand points, as well as introducing the energy dependence at the outset, insures the desired systematics. Work on this procedure is underway, and the relativistic Hartree constraint is being considered as one of the ways to parametrize the global optical potentials.[12]

IV. CONCLUSIONS

We have shown that Dirac optical model potentials whose real parts are constrained by relativistic Hartree calculations can be used to produce acceptable fits to proton-nucleus data over a wide range of energies for a number of spin-zero targets. This result provides a link between the phenomenology and the relativistic mean-field theory calculations, and indicates that the dominant energy dependence of the real optical potentials occurs simply as an overall scale. The model contains relatively few parameters and exhibits, in general, smooth energy dependence. These results also indicate that global parametrizations of the Dirac optical potential parameters are possible, and work towards this end is in progress.[12]

*Present address: Los Alamos National Laboratory, Group T-2, MS B-243, Los Alamos, NM 87545.

[1]C. J. Horowitz and B. D. Serot, Nucl. Phys. **A368**, 503 (1981).

[2]B. C. Clark, S. Hama, and R. L. Mercer, *The Interaction Between Medium Energy Nucleons in Nuclei (Indiana University Cyclotron Facility, Bloomington, Indiana)*, Proceedings of the Workshop on the Interactions Between Medium Energy Nucleons in Nuclei, AIP Conf. Proc. No. 97, edited by H. O. Meyer (AIP, New York, 1982), p. 260.

[3]L. G. Arnold, B. C. Clark, R. L. Mercer, and P. Schwandt, Phys. Rev. C **23**, 1949 (1981).

[4]L. D. Miller and A. E. S. Green, Phys. Rev. C **5**, 241 (1972); L. D. Miller, **9**, 537 (1974).

[5]J. D. Walecka, Ann. of Phys. **83**, 491 (1974).

[6]B. D. Serot, Phys. Lett. **86B**, 146 (1979); Erratum, Phys. Lett. **87B**, 403 (1979).

[7]M. E. Rose, *Relativistic Electron Theory* (Wiley, New York, 1961).

[8]R. L. Mercer, unpublished program CZENITH.

[9]E. D. Cooper, Ph.D. thesis, University of Alberta (1981), unpublished.

[10]References to the original sources for the intermediate energy data are given in P. Schwandt, *The Interaction Between Medium Energy Nucleons in Nuclei (Indiana University Cyclotron Facility, Bloomington, Indiana)*, Proceedings of the Workshop on the Interactions Between Medium Energy Nucleons in Nuclei, AIP Conf. Proc. No. 97, edited by H. O. Meyer (AIP, New York, 1982), p. 80.

[11]R. H. McCamis *et al.*, Phys. Rev. C **33**, 1624 (1986).

[12]E. D. Cooper, B. C. Clark, R. Kozack, S. Shim, S. Hama, J. I. Johansson, H. S. Sherif, R. L. Mercer, and B. D. Serot, Phys. Rev. C **36**, 2170 (1987).